Hindawi
Geofluids
Volume 2019, Article ID 8627698, 15 pages
https://doi.org/10.1155/2019/8627698

Research Article

Fluid Phase Simulation and Evolution of a Condensate Gas Reservoir in the Tazhong Uplift, Tarim Basin

Rui Deng,[1,2] Chengsheng Chen,[1,2] Shuyong Shi,[1,2] and Yunpeng Wang[1]

[1]*State Key Laboratory of Organic Geochemistry, Guangzhou Institute of Geochemistry, Chinese Academy of Sciences, Guangzhou 510640, China*
[2]*University of Chinese Academy of Sciences, Beijing 100039, China*

Correspondence should be addressed to Yunpeng Wang; wangyp@gig.ac.cn

Received 30 January 2019; Revised 1 May 2019; Accepted 27 May 2019; Published 13 June 2019

Academic Editor: Julien Bourdet

The fluid phase and the evolution of the condensate gas reservoir in the Lianglitage Formation (O_3), Well ZG7-5, Tazhong Uplift, were studied by integrating the PVTsim and the PetroMod software. The fluid phase was successfully simulated, and the burial, temperature, pressure, and pressure coefficient histories were reconstructed. The evolution of the fluid phase and its properties (density, viscosity, and gas-oil ratio) under the ideal and gas washing conditions was also explored. The simulated pressure-temperature (P-T) phase diagram confirms that the reservoir fluid is in the condensate gas phase at present, with an order of critical point-cricondenbar-cricondentherm (CP-P_m-T_m). The temperature and pressure show an overall increasing trend considering the entirety of geological evolution. Under ideal conditions, fluid transition from coexisting gas and liquid phases to a single condensate gas phase occurred during the Late Cretaceous (80 Ma, $T = 135.7^{\circ}$C, and $P = 58.19$ MPa). The density and viscosity of the liquid phase decreased gradually while the density and viscosity of the gas phase and the solution gas-oil ratio increased during geological processes. With the consideration of gas washing, the critical phase transition time points for 100% and 50% gas washing fluid are 394 Ma, 383 Ma, 331 Ma, and 23 Ma, as well as 266 Ma and 23 Ma, respectively. The average liquid phase density, gas phase density, and liquid phase viscosity under 100% gas washing are larger than those under 50% gas washing before 23 Ma (Miocene), while the gas phase viscosity values are similar for both cases. This study visually suggests that the temperature and pressure histories, which are controlled by the burial history and heat flow evolution, and gas washing have significant impacts on the formation of the condensate gas reservoirs and evolution of the fluid phase and its features in the Tazhong Uplift.

1. Introduction

The Tazhong Uplift is the most important oil and gas bearing area in the Tarim Basin of China. In recent decades, many different types of petroleum reservoirs have been discovered in the Tazhong Uplift, and the phase states of reservoir fluids vary among sand tar, super heavy oil, heavy oil, black oil, normal oil, light oil, condensate gas, and natural gas [1]. The condensate gas reservoirs serve as highly valued resources for energy supply, and their characteristic phase transitions during the accumulation and exploitation processes make them valuable for research [2].

Knowledge of the phase state and pressure-volume-temperature (PVT) properties of reservoir fluids is critical to the exploration and development of the reservoirs and, therefore, of interest in petroleum engineering studies [3, 4]. For all conventional and unconventional petroleum reservoirs, it is essential to reconstruct the phase evolution history and the changes in the gas-oil ratio (GOR) and physical properties of the fluid over time, which are all closely related to the burial and thermal histories of the fluid [5]. In many previous works, phase simulation experiments have been conducted under high temperature and pressure using PVT-based methods to obtain PVT properties and determine the phase types of reservoir fluids; however, such experiments are complicated, time-consuming, and difficult to conduct [6–10]. In addition, the fluid phase and evolution of condensate gas reservoirs in the Tazhong Uplift have not

been intensively studied; there is a lack of systematic studies on the temperature and pressure recoveries for condensate gas reservoirs in the area, as well as a lack of the combination with PVT simulation and basin modeling. Therefore, the purpose of this study was to explore the fluid phase and evolution of a typical condensate gas reservoir, Well ZG7-5, in the Tazhong Uplift. We first simulated the phase envelope and PVT properties of the fluids by using the PVTsim software, which is an easy-to-use and widely used software for the phase simulation of reservoir fluids. We then reconstructed the burial, temperature, pressure, and pressure coefficient evolution histories of the target reservoir using the PetroMod software. Finally, we studied the evolution of the fluid phase and its features (density, viscosity, and solution GOR) under ideal and gas washing conditions considering the entirety of geological evolution, by integrating the results of the PVTsim and the PetroMod software.

2. Geological Setting

The Tarim Basin, encompassing an area of 560,000 km^2, is the largest petroleum-bearing basin in China and is also one of the most complex superimposed basins in the world [11, 12]. This basin is characterized by thick sediments, multiple cycles of uplift and erosion, and complex distribution of oil and gas accumulations [13]. The Tazhong Uplift is a long-term inherited paleouplift in the central Tarim Basin, which was formed during the Caledonian orogeny and shaped by the Early Hercynian orogeny [14]; its tectonic framework did not significantly change during the subsequent Indosinian-Himalayan orogeny [15]. The oil and gas in the Tazhong Uplift are mainly distributed in the Cambrian, Ordovician, Silurian, and Carboniferous strata, and most condensate gas reservoirs are found in the Ordovician reservoirs originated from the Cambrian-Lower Ordovician strata and the Middle-Upper Ordovician source rocks [16]. The Tazhong Uplift can be subdivided into several belts including the Tazhong no. 1 fault zone, Tazhong no. 10 structural belt, Tazhong central horst belt, and Tazhong 1-8 buried hill belt [17, 18]. Well ZG7-5 is in the Tazhong no. 1 gas field and is located on the north slope of the Tazhong Uplift (Figure 1). The borehole depth of Well ZG7-5 reaches 5718 m, encountering strata from the Quaternary to the Ordovician. The condensate gas reservoir was discovered in the Lianglitage Formation (O_3, 5655-5718 m) where there is a daily gas production of 20399 m^3 but little oil production (inner report of the Tarim Oil Company, 2016).

3. Materials and Methods

3.1. Fluid Phase Simulation. The PVTsim software by the Calsep Company specializes in the calculation of fluid properties, employing several different equations of state (EOS); it is widely used in oil and gas reservoir studies [20]. The input data for the PVTsim software include well fluid components (C_1-C_{30+}, molecular weight), constant mass expansion experimental data, and constant volume depletion experimental data; these were all derived from the PVT analysis report for Well ZG7-5 (inner report of the Tarim Oil Company, 2016) (Tables 1 and 2). The data in the report were measured using a phase analyzer (Schlumberger DBR) and a gas chromatograph (Agilent 7890A, 6890N). The simulation steps are as follows: First, the well fluid components (C_1-C_{30+}, molecular weight) listed in Table 1 were input to the PVTsim software. The original *P-T* phase diagram showing the temperature and pressure of the critical point (CP), cricondentherm (T_m), and cricondenbar (P_m) was obtained after initially simulating with the Peng-Robinson equation of state (Figure 2(a)). Then, the relevant constant mass expansion experimental data and constant volume depletion experimental data listed in Table 2 were used to conduct a regression calculation. Afterward, the simulated values of CP, T_m, and P_m were tuned to achieve as much consistency as possible with the measured values by altering the parameters of EOS [21]. The final phase model was determined when the simulated *P-T* phase diagram was close to the measured one after repeated calculation and tuning; this simulated phase diagram was regarded as being representative of the actual fluid in the reservoir (Figure 2(b)). Additionally, the positional order of the critical point (CP), cricondentherm (T_m), cricondenbar (P_m), and in situ petroleum reservoir conditions (T_i, P_i) in the *P-T* phase diagram was used to identify the type of reservoir fluid.

3.2. One-Dimensional Basin Modeling

3.2.1. One-Dimensional Basin Modeling Method. The temperature and pressure histories of the Lianglitage Formation (O_3), Well ZG7-5, were determined by reconstructing a geological model using the PetroMod 2016 (1D) software by Schlumberger Limited. The input parameters for this purpose include stratigraphy (age, thickness, and lithology), tectonic events (unconformities, erosion time, and erosion thickness), and boundary conditions (heat flow, paleowater depth, and sediment-water interface temperature) [22–24]. During the simulation process, the measured temperature and maturity values were used to validate the modeling results. The burial, temperature, pressure, and pressure coefficient evolution histories of the target reservoir were confirmed when the modeled and measured results were consistent.

3.2.2. Input Data for One-Dimensional Basin Modeling. Erosion events have a significant influence on both the burial and thermal histories. The modeled stratigraphic succession of Well ZG7-5 starts from the Quaternary and continues down to the Lianglitage Formation (Ordovician), excluding the Jurassic, Devonian, and Upper Silurian strata which show the effects of multiple tectonic events. The concrete values of erosion thickness and erosion time were collected from Zhang et al. [25], Pang et al. [26], and Qi and Liu [27]. The main deposition and erosion events are listed in Table 3. The data for stratigraphy (age, thickness, and lithology) were gathered from the logging report from the Tarim Oil Company.

In terms of the boundary conditions, the heat flow values are vital to unearthing the reservoir thermal maturity history. Values of heat flow were derived from Qiu et al. [28], Wang et al. [29], and Feng et al. [30]. The values of the paleowater

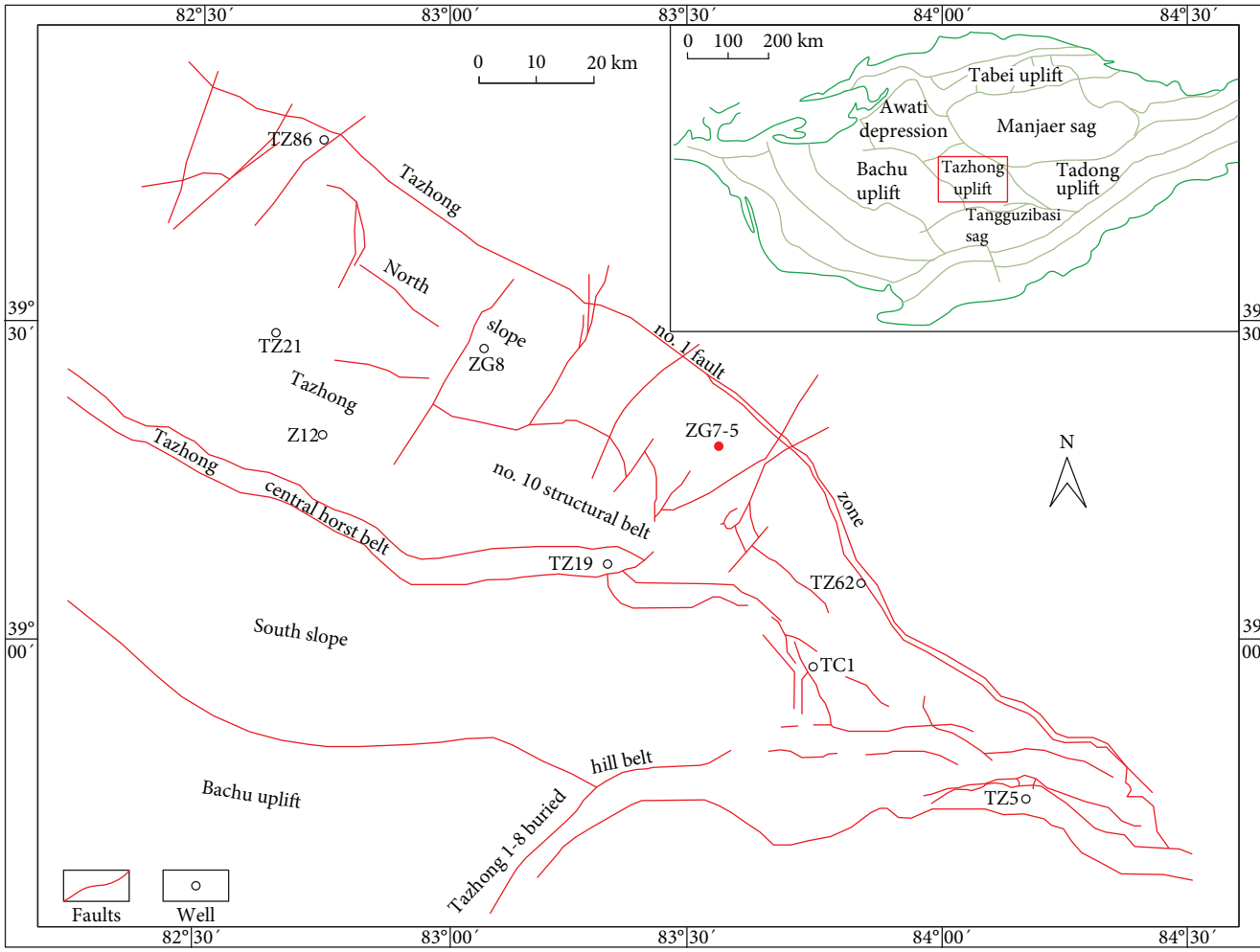

Figure 1: Map showing the location of Well ZG7-5 and the geological structures in the Tazhong Uplift (modified from [19]).

Table 1: Well fluid components (C_1-C_{30+}) of the Lianglitage (O_3) reservoir in Well ZG7-5.

Components	Mol%	Molecular weight	Components	Mol%	Molecular weight
N_2	4.232	28.014	C_{14}	0.334	190
CO_2	3.075	44.01	C_{15}	0.260	206
C_1	83.083	16.043	C_{16}	0.177	222
C_2	0.364	30.07	C_{17}	0.143	237
C_3	0.206	44.097	C_{18}	0.118	251
iC_4	0.078	58.124	C_{19}	0.102	263
nC_4	0.203	58.124	C_{20}	0.091	275
iC_5	0.147	72.151	C_{21}	0.089	291
nC_5	0.172	72.151	C_{22}	0.085	305
C_6	0.280	86.178	C_{23}	0.075	318
C_7	0.315	96	C_{24}	0.059	331
C_8	1.645	107	C_{25}	0.054	345
C_9	1.374	121	C_{26}	0.041	359
C_{10}	1.135	134	C_{27}	0.024	374
C_{11}	0.867	147	C_{28}	0.014	388
C_{12}	0.624	226	C_{29}	0.007	402
C_{13}	0.518	175	C_{30+}	0.011	416

Table 2: Experimental data for constant mass expansion and constant volume depletion.

Well	Constant mass expansion experiment			Constant volume depletion experiment		
	Pressure (MPa)	Temperature (°C)	Liquid vol% of Vd	Pressure (MPa)	Temperature (°C)	Z factor gas
ZG 7-5	61.46*	102.6	0.00			
	59.16*	122.6	0.00	56.81	142.6	1.374
	56.81*	142.6	0.00			

*Dew point pressure.

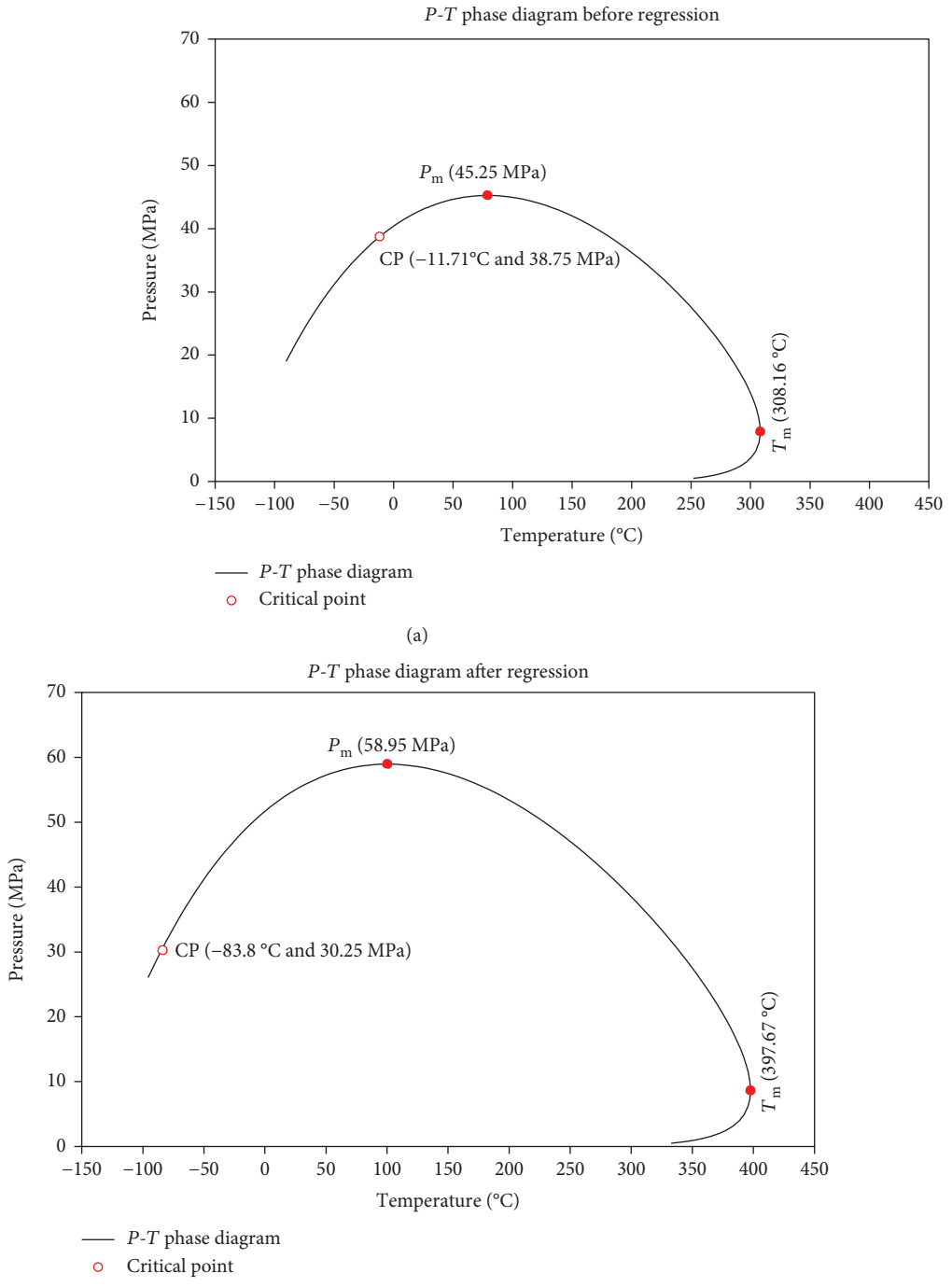

Figure 2: The original P-T phase diagram (before regression) and the final P-T phase diagram (after regression).

Table 3: The main deposition and erosion events in Well ZG7-5.

Age (Ma)	Strata	Depth (m)	Erosion thickness (m)	Lithology
0	Top N+Q	0		Sandstone, shale
23	Top E	1200		Sandstone
66	Top K	1834		Sandstone, shale
144	Erosion J		-150	
163	Top J		150	Sandstone, shale
201	Top T	2390		Shale, siltstone, conglomerate
247	Erosion P		-150	
254	Top P	2906	150	Shale, siltstone, conglomerate
298.9	Top C	3562		Shale, sandstone, limestone
358	Erosion D		-700	
387	Top D		700	Sandstone
417.6	Erosion S		-100	
427.4	Top S	4140	100	Sandstone, shale, siltstone
442	Erosion O_3s		-900	
443	Top O_3s	4482	900	Shale
453.4	Top $O_3l_{1\text{-}2}$	5333		Limestone, sandstone
454.9	Target layer	5457		Limestone
458	Erosion O_1ys		-250	
459.9	Erosion O_2yif		-100	
460.7	Erosion O_2t		-50	
461	Top O_2t		50	Limestone
464.7	Top O_2yjf		100	Limestone
470	Top O_1ys	5711	250	Limestone, dolomite
479.5	Top O_1p	6261		Dolomite, limestone
485.4	Base	6761		

depth (PWD) were estimated by sedimentary facies type and lithology, which are closely related to variations in the global sea level. The sediment-water interface temperatures (SWIT) were calculated using the PetroMod software upon identification of the location of the well. The plots for the concrete boundary conditions are presented in Figure 3. The temperature and maturity values measured for calibration were taken from the logging report and laboratory measurements by the Tarim Oil Company.

Finally, evolution of the fluid phase and its features (density, viscosity, and solution GOR) under ideal and gas washing conditions was studied by integrating the phase diagram from running the PVTsim software and the temperature-pressure values at each critical geological event point, derived by the PetroMod software.

4. Results and Discussion

4.1. P-T Phase Diagram for the Fluid. As mentioned above, the final phase diagram for the fluid was arrived at after several rounds of calculation and tuning, and the corresponding fluid features were calculated. Table 4 presents a comparison between the simulated and measured values of the fluid features of Well ZG7-5. The modeled features are consistent with the measured results. Further, the modeled density of oil on the ground and the solution GOR show relatively large errors because oil density was measured with the loss of some light fractions, and the produced GOR, which slightly differs from the solution GOR, was measured. These comparisons illustrate that the modeling results are valid and the method is effective. The simulated *P-T* phase diagram for the fluids in the Lianglitage reservoir (O_3) is displayed in Figure 4. It can be seen that the temperature and pressure of the critical point (CP) are -83.8°C and 30.25 MPa, respectively, and the cricondentherm (T_m) and cricondenbar (P_m) are 397.67°C and 58.95 MPa, respectively. Furthermore, the *P-T* phase diagram is divided into the liquid phase zone, the condensate gas phase zone, the gas phase zone, and the coexistence phase zone for gas and liquid, by the positional order of the critical point (CP), cricondentherm (T_m), and cricondenbar (P_m). Based on the phase zone distribution of the *P-T* diagram and the in situ reservoir conditions ($T_i = 143.3$°C, $P_i = 91.66$ MPa), the in situ reservoir fluid was classified as being of the condensate gas phase type. Under the conditions of normal temperature and pressure (20°C, 0.101 MPa), the fluid returns from the condensate gas phase to two separate phases of gas and liquid, which coincides with the current product type and macro compositions.

4.2. Histories of Burial, Temperature, Pressure, and Pressure Coefficient. As can be seen from Figure 5, the measured and modeled values of temperature and vitrinite reflectance

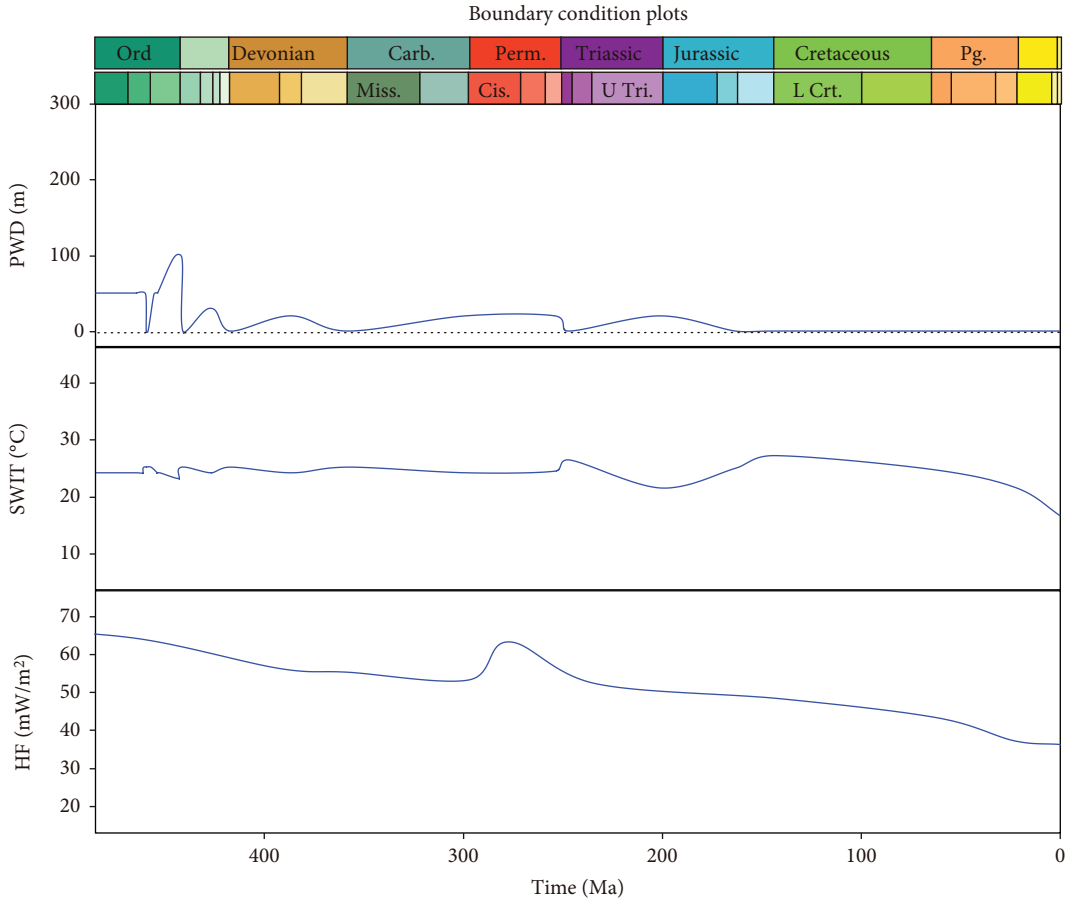

Figure 3: The boundary condition plots for Well ZG7-5.

Table 4: Comparison between simulated and measured features of the fluid.

Items	Simulated values	Measured values
Critical temperature (°C)	-83.80	-77.80
Critical pressure (MPa)	30.25	29.25
Cricondentherm (°C)	397.67	386.30
Cricondenbar (MPa)	58.95	57.71
Dew point pressure(142.6°C) (MPa)	58.00	56.81
Oil density at ground(20°C) (g/cm^3)	0.72	0.80*
Solution gas-oil ratio (GOR) (m^3/m^3)	883	823**

*Measured with some loss of volatile fractions. **Produced GOR.

(Ro) fit well, indicating the reliability of burial, temperature, pressure, and pressure coefficient histories modeled using the PetroMod software.

The burial history overlaying with the thermal maturity history of Well ZG7-5 is shown in Figure 6, which indicates that the Tazhong Uplift has experienced multiple stages of uplift and erosion caused by multiple orogenies. Among all these orogenies, the Caledonian and Hercynian orogenies had the most crucial impact on the study area. The Tarim Basin experienced a period of stable platform development during the Cambrian-Early Ordovician and encountered a slight erosion during the Late Middle Ordovician. Subsequently, the rapid subsidence and the following strong erosion of strata caused by the Middle Caledonian orogeny were the significant features of the Late Ordovician. This orogeny was also characterized by the strongest uplift and erosion (900 m) during the entire geological evolution history in the study area. During the Late Devonian, the Hercynian orogeny caused another strong uplift and erosion (700 m). The combined Caledonian and Hercynian orogenies caused an erosion thickness of more than 2000 m, and the Ordovician strata reached high-mature states (1.3-2.0%Ro) at the beginning of the Permian period. The orogeny events following this period had little impacts on the maturity. Currently, the Ordovician strata are buried to the maximum depth of over 6000 m.

Figure 7 shows the temperature and pressure histories of the Lianglitage Formation (O_3) in Well ZG7-5. The temperature history is significantly linked with the heat flow evolution and the burial history, while the pressure history is correlated with the burial history and lithology. Both the temperature and pressure histories depict overall increasing trends from the Ordovician to the present; however, decreasing trends caused by erosion events, heat flow

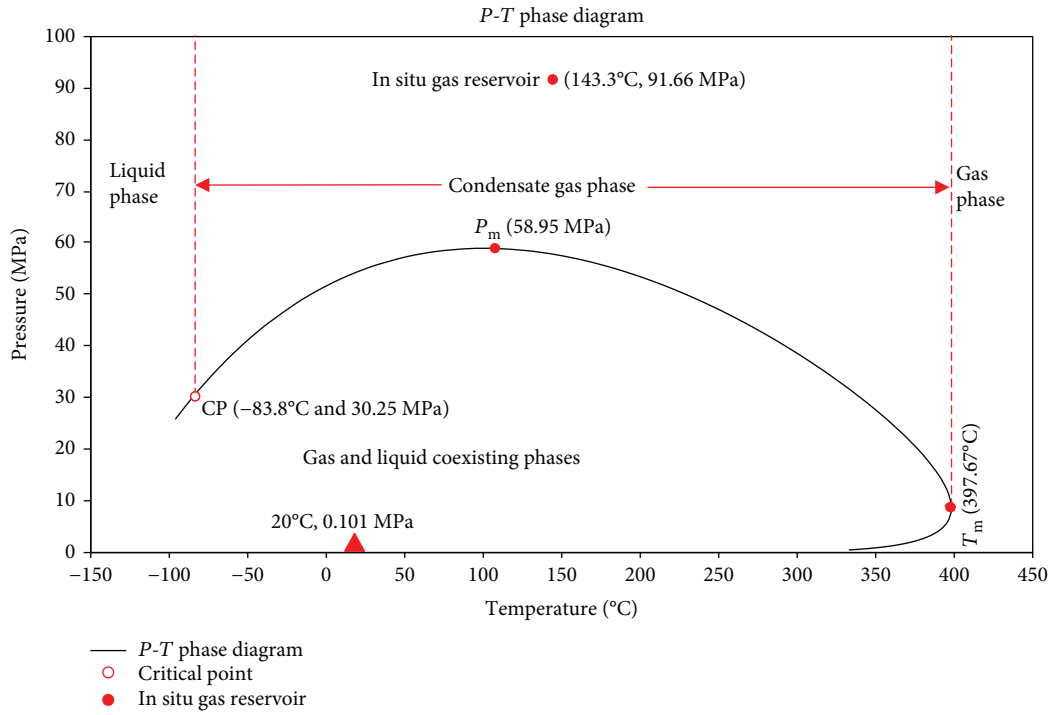

Figure 4: *P-T* phase diagram for the fluid in Well ZG7-5.

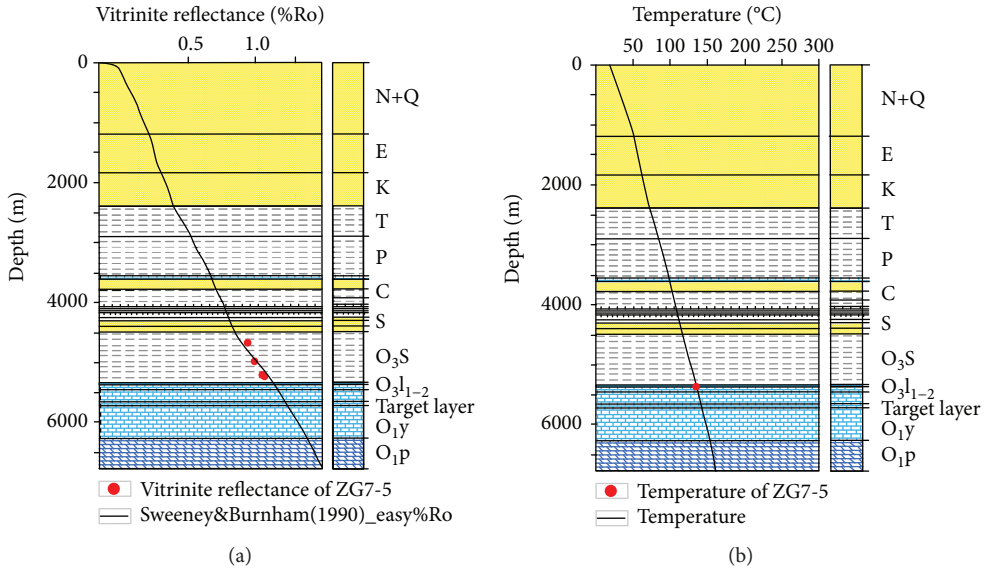

Figure 5: Good fit between the measured temperature and maturities and the modeled results of Well ZG7-5.

changes, or lithology variations were also observed. Moreover, the pressure coefficients throughout the evolution history were also calculated by the results derived from PetroMod (Figure 8). During the early stages, the reservoir was in normal pressure condition; these conditions changed to the state of overpressure (pressure coefficient > 1.2) during the Middle Permian (265 Ma) due to the deepening of the burial depth. After the Miocene, the pressure coefficient increased rapidly.

4.3. The Evolution of the Fluid Phase and Features

4.3.1. Ideal Conditions. Under ideal conditions, we assumed that the reservoir was formed without any destruction or change and the composition of the reservoir fluid was constant during the entire geological process. The simulated phase envelope and the modeled temperature-pressure values (labeled as the *P-T* line) at each time point of a critical geological event were overlapped in the same plot to

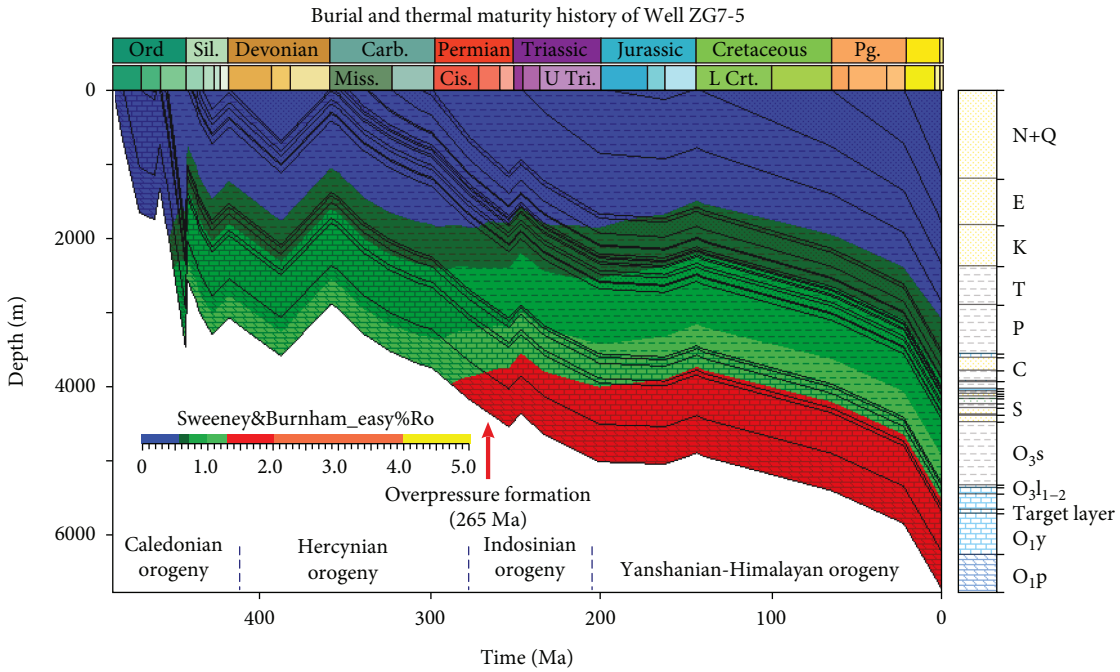

FIGURE 6: The burial history overlaying the thermal maturity history of Well ZG7-5.

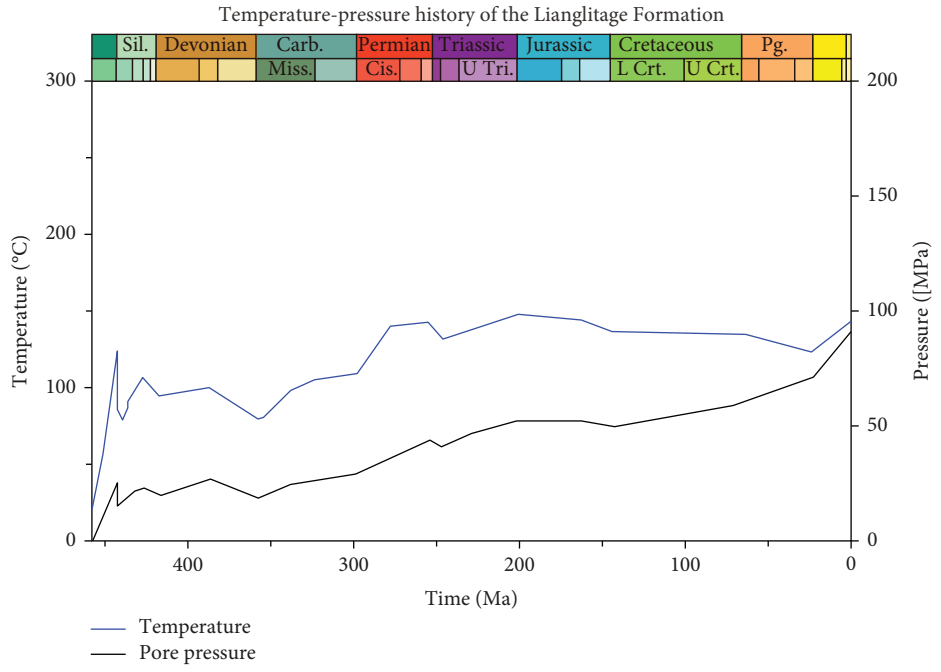

FIGURE 7: Temperature (T) and pressure (P) histories (upper) of the Lianglitage Formation (O_3) in Well ZG7-5.

investigate the reservoir evolution processes (Figure 9). The figure clearly shows that the P-T line goes across the coexisting phase zone of the gas and liquid to the condensate gas phase zone and the turning point (135.7°C, 58.19 MPa) corresponding to the age of 80 Ma (Late Cretaceous) appears at the point of intersection of the two lines. This suggests that the Lianglitage Formation (O_3) existed in the two-phase states of gas and liquid from Ordovician to 80 Ma (Late Cretaceous) but, thereafter, turned to the condensate gas phase. This phenomenon clearly indicates that the condensate gas reservoir was formed after 80 Ma (Late Cretaceous) due to the changes in temperature and pressure conditions, which, in turn, were the result of the combined effect of multiple orogenies (the change of burial depth), as well as the heat flow evolution.

The changes in temperature and pressure controlled by heat flow evolution and multiple orogenies also affected fluid

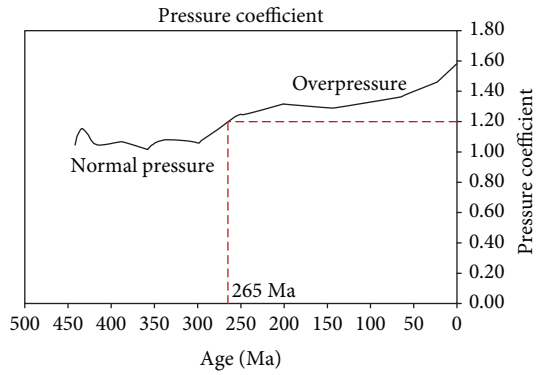

Figure 8: The pressure coefficient evolution of the Lianglitage Formation (O_3) in Well ZG7-5.

features. The evolutions of density, viscosity, and solution GOR during the entire geological processes are presented in Figure 10. From Ordovician to 80 Ma (Late Cretaceous), the fluid in the reservoir was composed of coexisting gas and liquid phases. The density of the liquid phase decreased gradually, while that of the gas fluctuated greatly and generally increased. On the contrary, the viscosity of the liquid phase fluctuated greatly, showing an overall decreasing trend and that of gas gradually increased. The fluctuations in density and viscosity are synchronized with the wave of burial depth. After 80 Ma (Late Cretaceous), the fluid turned into the condensate gas phase with increasing temperature and pressure. At the same time, the density and viscosity of the gas continually increased to reach the present values of 0.44 g/cm^3 and 0.0693 cP, respectively (Figures 10(a) and 10(b)). In the solution GOR, the amount of gas increased continuously; an increasing number of liquid hydrocarbons underwent the retrograde evaporation processes with continuous deep burial. This led the solution GOR to depict an overall increasing trend throughout the well-formation history; its value eventually reached 883 m^3/m^3 (Figure 10(c)). As mentioned above, after the Middle Permian (265 Ma), the overpressure state dominated the reservoir environment and the pressure coefficient increased rapidly after the Miocene. It is believed that the fluid expansion caused by retrograde evaporation is the main reason for the formation of overpressure. Moreover, the changes in pressure coefficient are also indirectly related with the alterations in GOR.

4.3.2. Gas Washing Conditions. From previous studies, it is known that oil charging occurred mainly in the Late Caledonian and Late Hercynian periods and that the gas filling that occurred mostly during the Late Himalayan period is one of the formation mechanisms of the condensate gas reservoirs in the Tazhong area [31]. In this context, it is hypothesized that the condensate gas reservoir of Well ZG7-5 was formed due to gas washing during the Late Himalayan. This assumes two different gas washing conditions: one, that the initial methane content is 0% (before being normalized) and that all the methane was a product of gas washing; therefore, the degree of gas washing can be set to 100%; the other is that half the methane (before being normalized) was from gas washing, and therefore, the gas washing degree can be set to 50%. The specific fluid components (C_1-C_{30+}) for these two cases are listed in Table 5 (only the amount of methane was varied; the other components were kept constant). We also assumed that 23 Ma (Late Himalayan) was the time at which the gas washing occurred, based on previous studies [32, 33]. The methods described above were then used to study the process of evolution with gas washing. The fluid phase evolution diagram of the Lianglitage Formation (O_3) in Well ZG7-5, considering gas washing, is shown in Figure 11. The *P-T* phase diagram in Figure 4 was also plotted in Figure 11 to represent the final *P-T* phase diagram of the gas-washed fluid.

In the 100% gas washing case, its initial phase diagram stayed in the high temperature and low pressure area because of the limited gas content and its critical point is 344.19°C and 11.79 MPa (Figure 11(a)). The fluid clearly existed as two phases, gas and liquid, from the Ordovician to the Middle Devonian (394 Ma). The fluid then transitioned quickly to the liquid phase before 383 Ma (Middle Devonian) and returned to the two-phase state again due to the changes in temperature and pressure conditions. After 331 Ma (Early Carboniferous), the fluid stayed in the liquid phase but turned into the condensate gas phase with gas washing in 23 Ma (Miocene) (Figure 11(a)).

There are some differences in the phase transition of the fluid when 50% of the gas was washed compared to when 100% of the gas was washed. The initial phase diagram of the former is in a lower temperature and higher pressure area compared to the latter because of its higher gas content, and its critical point is 149.09°C and 40.59 MPa (Figure 11(b)). The phase of the fluid remained in the two-state phase from the Ordovician to the Middle Permian (266 Ma), lasting longer than in the 100% gas washing case. Then, from 266 to 247 Ma (Middle Permian-Early Triassic), the fluid stayed in the liquid phase, with only a brief transition to the two-state phase. Finally, the fluid transitioned from the liquid phase to the condensate gas phase after gas washing in 23 Ma (Miocene). The occurrence time of the gas phase in the 50% gas washing case is longer than the 100% gas washing case. Thus, the critical phase turning time points for the 100% and 50% gas-washed fluid are 394, 383, 331, and 23 Ma, as well as 266 and 23 Ma, respectively.

The evolution of fluid density and viscosity in these two cases was also studied using the methods described above, and the results are shown in Figure 12. The figure also clearly shows the change of phase state. In the 100% gas washing case, the density of the liquid phase remained basically the same, fluctuating slightly in the 0.69-0.73 g/cm^3 range, while the gas phase existed for a shorter time but had values that changed more obviously (Figure 12(a)). Conversely, there was great fluctuation in the viscosity of the liquid phase but little fluctuation in the gas phase viscosity (Figure 12(b)).

In the 50% gas washing case, the fluctuations in density and viscosity were greater than those of the 100% gas washing case (Figures 12(c) and 12(d)). The density of the liquid phase first fluctuated greatly, with an overall decreasing trend, and then gradually increased. The density of the gas phase shows an increasing trend throughout. The sharp

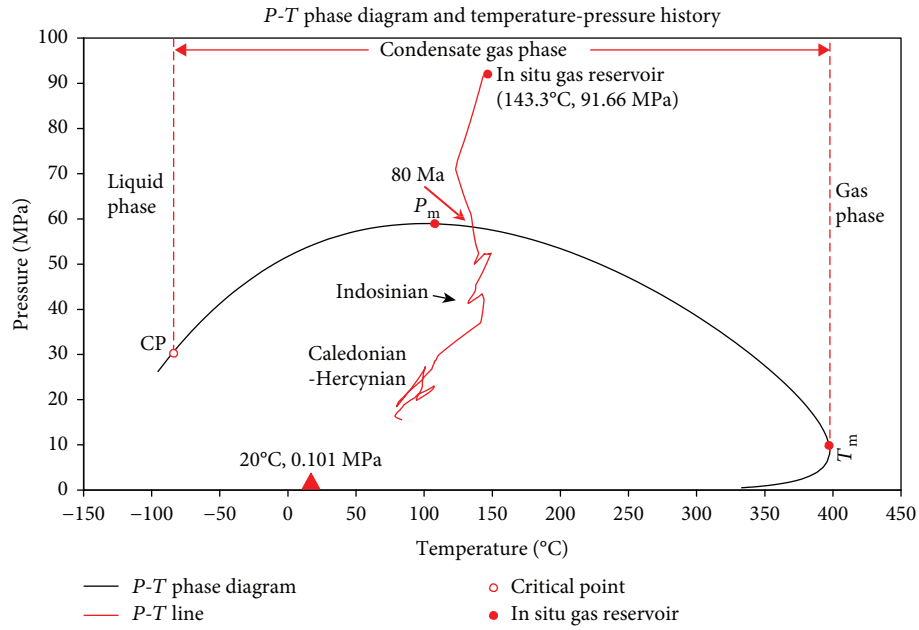

Figure 9: The fluid phase evolution diagram of the Lianglitage Formation (O_3) in Well ZG7-5 (under ideal conditions).

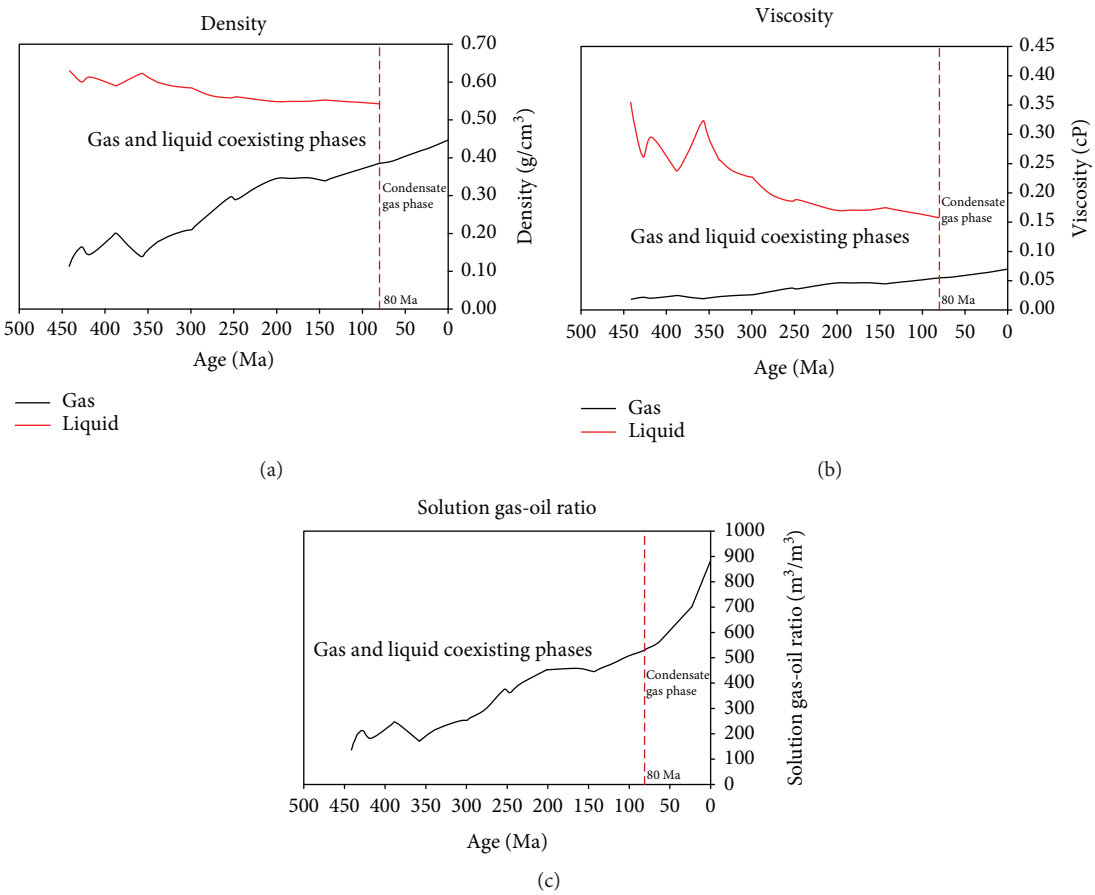

Figure 10: The evolution of fluid density, viscosity, and solution gas-oil ratio (GOR) under ideal conditions.

changes between 350 and 266 Ma (Early Carboniferous-Middle Permian) are believed to have been caused by the continuous burial and the high heat flow value during the Carboniferous and Permian (Figure 12(c)) [34, 35]. The viscosity of the liquid phase also changed greatly while the viscosity of the gas phase increased gradually (Figure 12(d)).

Table 5: The specific well fluid components (C_1-C_{30+}) of different gas washing degrees.

Gas washing degree	Components (%) (after normalized)																
100%	N_2	CO_2	C_1	C_2	C_3	iC_4	nC_4	iC_5	nC_5	C_6	C_7	C_8	C_9	C_{10}	C_{11}	C_{12}	C_{13}
	25.013	18.175	0.000	2.151	1.218	0.461	1.200	0.869	1.017	1.655	1.862	9.723	8.121	6.708	5.124	3.688	3.062
	C_{14}	C_{15}	C_{16}	C_{17}	C_{18}	C_{19}	C_{20}	C_{21}	C_{22}	C_{23}	C_{24}	C_{25}	C_{26}	C_{27}	C_{28}	C_{29}	C_{30+}
	1.974	1.537	1.046	0.845	0.697	0.603	0.538	0.526	0.502	0.443	0.349	0.319	0.242	0.142	0.083	0.041	0.065
50%	N_2	CO_2	C_1	C_2	C_3	iC_4	nC_4	iC_5	nC_5	C_6	C_7	C_8	C_9	C_{10}	C_{11}	C_{12}	C_{13}
	7.250	5.268	71.014	0.624	0.353	0.134	0.348	0.252	0.295	0.480	0.540	2.818	2.354	1.945	1.485	1.069	0.887
	C_{14}	C_{15}	C_{16}	C_{17}	C_{18}	C_{19}	C_{20}	C_{21}	C_{22}	C_{23}	C_{24}	C_{25}	C_{26}	C_{27}	C_{28}	C_{29}	C_{30+}
	0.572	0.445	0.303	0.245	0.202	0.175	0.156	0.152	0.146	0.128	0.101	0.093	0.070	0.041	0.024	0.012	0.019

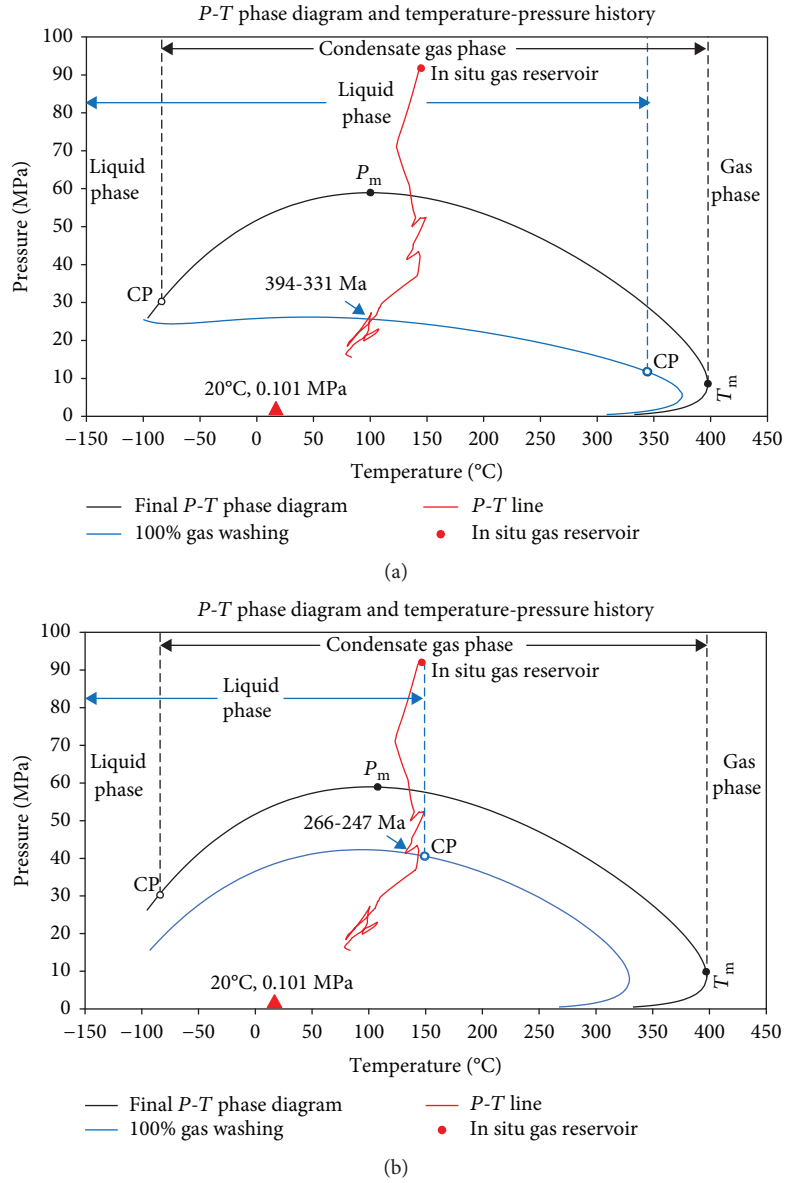

Figure 11: The phase evolution diagram of the fluid in the Lianglitage Formation (O_3) in Well ZG7-5, taking gas washing into account.

In general, the average liquid and gas phase densities and the liquid phase viscosity of the 50% gas washing case are smaller than those of the 100% gas washing case before 23 Ma (Miocene), whereas their gas phase viscosity values are similar. These results indicate that the degree of gas washing has a great impact on the fluid phase, phase transition point, and fluid features.

5. Conclusions

The simulated *P-T* phase diagram confirms that the studied reservoir is presently in the condensate gas phase, in the order CP-P_m-T_m. The modeled burial history shows that the Tazhong Uplift experienced multiple stages of uplift and erosion caused by multiple orogenies. The modeled temperature and pressure histories influenced by the burial history and the evolution of the heat flow show an overall increasing trend from the Ordovician to the present. The reservoir experienced overpressure after the Middle Permian (265 Ma) because of the increasing pressure caused by the continuous subsidence; the pressure coefficient also increased rapidly after the Miocene.

Under ideal conditions, the reservoir fluid was assumed to have formed without any destruction or change. The simulated results show that 80 Ma (Late Cretaceous, $T = 135.7°C$, $P = 58.19$ MPa) was a key point in the phase transition from the two-state gas and liquid phases to the single-state condensate gas phase that led to the formation of the present condensate gas reservoir. The density and viscosity of the liquid phase decreased gradually while the density and viscosity of the gas phase increased with the increasing temperature and pressure during geological processes. The solution GOR increased throughout the history of the reservoir and eventually reached 883 m^3/m^3.

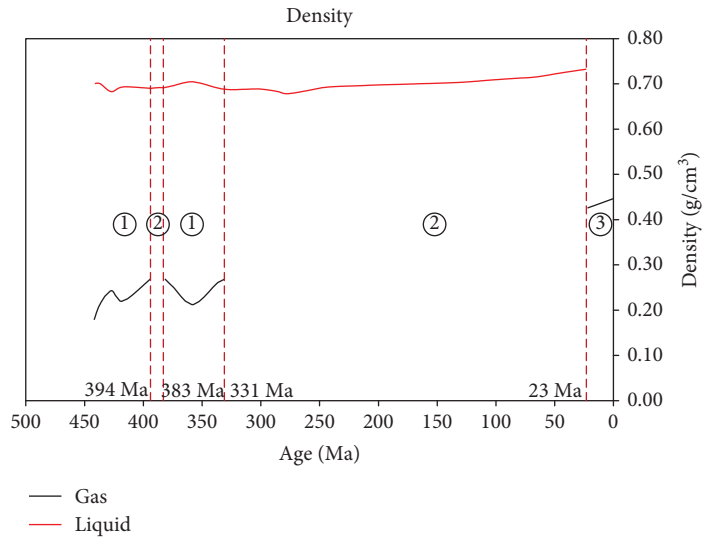

(a)

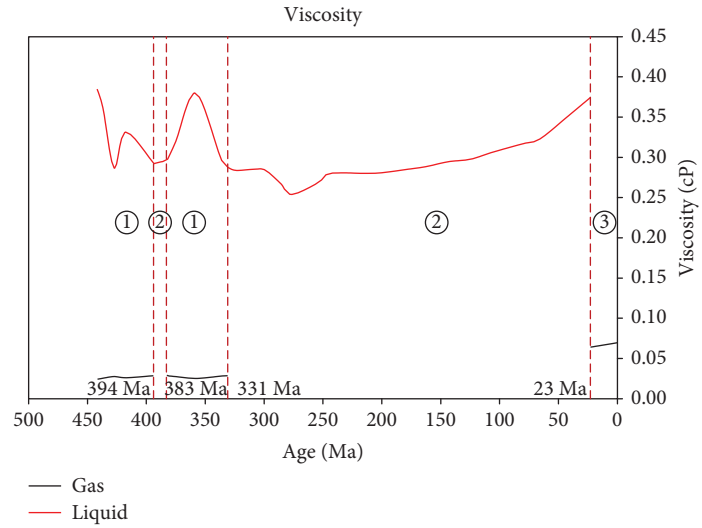

(b)

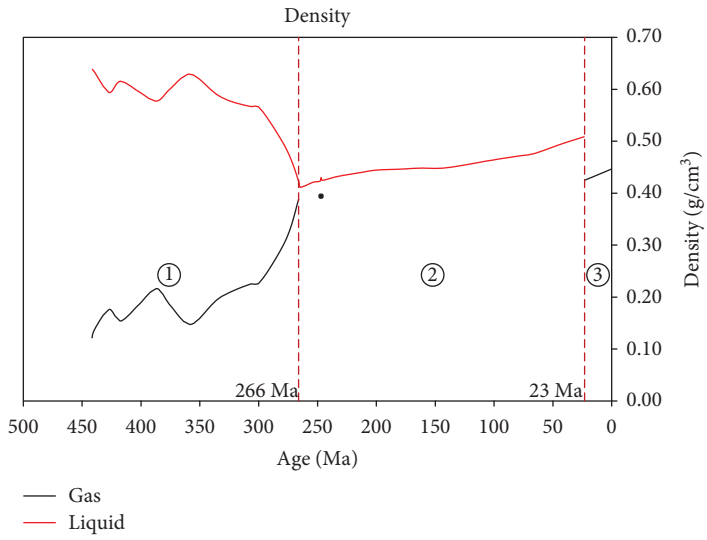

(c)

Figure 12: Continued.

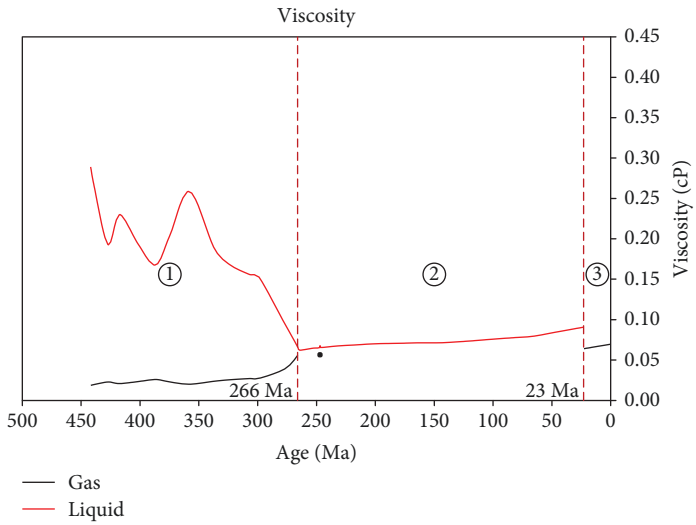

Figure 12: The evolution of the density and viscosity of the fluid in the Lianglitage Formation, taking gas washing into account. (a, b) 100% gas washing degree; (c, d) 50% gas washing degree. ①: coexisting gas and liquid phases; ②: liquid phase; and ③: condensate gas phase.

Taking the gas washing into consideration, it is hypothesized that the condensate gas reservoir was formed due to gas washing that occurred in the Late Himalayan (23 Ma). The simulations of gas washing degrees of 100% and 50% were designed to study how the gas washing affected the evolutionary history of the fluid phase. The results show that the critical time points in the change in the 100% and 50% gas washing cases are 394, 383, 331, and 23 Ma, as well as 266 and 23 Ma, respectively. The average liquid and gas phase densities and the liquid phase viscosity of the 100% gas washing case are greater than those of the 50% gas washing case before 23 Ma (Miocene). The gas phase viscosity of the two cases is similar.

The formation of condensate gas reservoirs in the Tazhong Uplift is associated not only with the changes in temperature and pressure controlled by burial history and the evolution of heat flow but also with the gas washing that occurred during the Late Himalayan, which played a critical role in forming the condensate gas reservoirs. This study confirms that both of these processes could result in the formation of condensate gas reservoirs. Moreover, it indicates that the method of integrating the PVTsim and the PetroMod software to study the phase simulations and evolution of a reservoir is useful and effective.

Data Availability

The data used to support the findings of this study are available from the corresponding author upon request.

Conflicts of Interest

The authors declare that there are no conflicts of interest regarding the publication of this paper.

Acknowledgments

This work was supported by the Strategic Priority Research Program of the Chinese Academy of Sciences (XDA14010103), the China National Major S&T Program (2017ZX05008-002-030), the GIG 135 Project (No. 135TP201602), and the NSFC Project (41372137). This is contribution No. IS-2716 from the Guangzhou Institute of Geochemistry, Chinese Academy of Sciences.

References

[1] S. Zhang, G. Zhu, H. Yang et al., "The phases of Ordovician hydrocarbon and their origin in the Tabei uplift, Tarim Basin," *Acta Petrologica Sinica*, vol. 27, no. 8, pp. 2447–2460, 2011.

[2] H. Yang and G. Zhu, "The condensate gas field geological characteristics and its formation mechanism in Tarim Basin," *Acta Petrologica Sinica*, vol. 29, no. 9, pp. 3233–3250, 2013.

[3] S. Zendehboudi, M. A. Ahmadi, L. James, and I. Chatzis, "Prediction of condensate-to-gas ratio for retrograde gas condensate reservoirs using artificial neural network with particle swarm optimization," *Energy & Fuels*, vol. 26, no. 6, pp. 3432–3447, 2012.

[4] E. Ganji-Azad, S. Rafiee-Taghanaki, H. Rezaei, M. Arabloo, and H. A. Zamani, "Reservoir fluid PVT properties modeling using adaptive neuro-fuzzy inference systems," *Journal of Natural Gas Science and Engineering*, vol. 21, pp. 951–961, 2014.

[5] J. Tan, B. Horsfield, N. Mahlstedt et al., "Physical properties of petroleum formed during maturation of Lower Cambrian shale in the upper Yangtze Platform, South China, as inferred from PhaseKinetics modelling," *Marine and Petroleum Geology*, vol. 48, pp. 47–56, 2013.

[6] R. Di Primio, V. Dieckmann, and N. Mills, "PVT and phase behaviour analysis in petroleum exploration," *Organic Geochemistry*, vol. 29, no. 1-3, pp. 207–222, 1998.

[7] Z. Xingxi, W. Hongjun, C. Yicai, and X. Zhiming, "The study on the contributing factors of phase state of gas condensate:

examples from Tarim Basin," *Marine and Petroleum Geology*, vol. 15, no. 1, pp. 21–31, 1998.

[8] H. Zhang, S. Zhou, D. Fu et al., "Petroleum phase state prediction in deep reservoir of Tashen-1 well in Tarim Basin," *Natural Gas Geoscience*, vol. 24, no. 5, pp. 999–1004, 2013.

[9] Y. Tan, Y. Jiang, L. Zhao, X. Mu, and T. Xu, "Main controlling factors of phase evolution and charging pattern of hydrocarbons in northern Dongpu sag," *Petroleum Geology & Experiment*, vol. 37, no. 1, pp. 28–34, 2015.

[10] S. Cui, H. Gu, S. Fang, and W. Yu, "Full component simulation of condensate gas in well Chunxiao 3 in Donghai oilfield," *Petroleum Geology and Recovery Efficiency*, vol. 9, no. 1, pp. 54–56, 2002.

[11] L. Desheng, L. Digang, J. Chengzao, W. Gang, W. Qizhi, and H. Dengfa, "Hydrocarbon accumulations in the Tarim Basin, China," *AAPG Bulletin*, vol. 80, no. 10, pp. 1587–1603, 1996.

[12] G. Zhu, A. V. Milkov, F. Chen et al., "Non-cracked oil in ultra-deep high-temperature reservoirs in the Tarim Basin, China," *Marine and Petroleum Geology*, vol. 89, pp. 252–262, 2018.

[13] C. Jia, *Tectonic Characteristics and Petroleum, Tarim Basin*, Petroleum Industry Press, China, 1997.

[14] H. Pang, J. Chen, X. Pang et al., "Analysis of secondary migration of hydrocarbons in the Ordovician carbonate reservoirs in the Tazhong uplift, Tarim Basin, China," *AAPG Bulletin*, vol. 97, no. 10, pp. 1765–1783, 2013.

[15] S. Li, X. Pang, Z. Jin et al., "Petroleum source in the Tazhong uplift, Tarim Basin: new insights from geochemical and fluid inclusion data," *Organic Geochemistry*, vol. 41, no. 6, pp. 531–553, 2010.

[16] Q. Liu, Z. Jin, H. Li et al., "Geochemistry characteristics and genetic types of natural gas in central part of the Tarim Basin, NW China," *Marine and Petroleum Geology*, vol. 89, pp. 91–105, 2018.

[17] X. Zhou, X. Pang, Q. Li et al., "Advances and problems in hydrocarbon exploration in the Tazhong area, Tarim Basin," *Petroleum Science*, vol. 7, no. 2, pp. 164–178, 2010.

[18] J. Chen, X. Pang, and Z. Jiang, "Controlling factors and genesis of hydrocarbons with complex phase state in the upper Ordovician of the Tazhong area, Tarim Basin, China," *Canadian Journal of Earth Sciences*, vol. 52, no. 10, pp. 880–892, 2015.

[19] Y. Zhang, X. Lyu, H. Yu, B. Jing, C. Zhang, and J. Cai, "Controlling mechanism of two strike-slip fault groups on the development of the Ordovician karst reservoirs in the Tazhong uplift, Tarim Basin," *Oil & Gas Geology*, vol. 37, no. 5, pp. 663–673, 2016.

[20] P. Dimitrakopoulos, W. Jia, and C. Li, "An improved computational method for the calculation of mixture liquid–vapor critical points," *International Journal of Thermophysics*, vol. 35, no. 5, pp. 865–889, 2014.

[21] W. A. England, "Empirical correlations to predict gas/gas condensate phase behaviour in sedimentary basins," *Organic Geochemistry*, vol. 33, no. 6, pp. 665–673, 2002.

[22] X. Yao and Y. Wang, "Assessing shale gas resources of Wufeng-Longmaxi shale (O3w-S1l) in Jiaoshiba area, SE Sichuan (China) using PetroMod I: burial and thermal histories," *Petroleum Science and Technology*, vol. 34, no. 11-12, pp. 1000–1007, 2016.

[23] M. Mei, K. K. (. A.). Bissada, T. B. Malloy, L. M. Darnell, and Z. Liu, "Origin of condensates and natural gases in the Almond Formation reservoirs in southwestern Wyoming, USA," *Organic Geochemistry*, vol. 124, pp. 164–179, 2018.

[24] C. Shangbin, Z. Yanming, C. Si, H. Yufu, F. Changqing, and F. Junhua, "Hydrocarbon generation and shale gas accumulation in the Longmaxi Formation, southern Sichuan Basin, China," *Marine and Petroleum Geology*, vol. 86, pp. 248–258, 2017.

[25] Y. Zhang, Z. Jin, G. Liu, and J. Li, "Study on the formation of unconformaties and the amount of the eroded sedimentation in the Tarim Basin," *Earth Science Frontiers*, vol. 7, no. 4, pp. 449–457, 2000.

[26] X. Pang, C. Jia, H. Pang, and H. Yang, "Destruction of hydrocarbon reservoirs due to tectonic modifications: conceptual models and quantitative evaluation on the Tarim Basin, China," *Marine and Petroleum Geology*, vol. 91, pp. 401–421, 2018.

[27] Y. Qi and G. Liu, "Wave process analysis and erosion thickness study of unconformities in the sedimentary basin: examples of the Tarim Basin, Xinjiang," *Journal of Jiaozuo Institute of Technology*, vol. 18, no. 3, pp. 161–165, 1999.

[28] N. Qiu, J. Chang, Y. Zuo, J. Wang, and H. Li, "Thermal evolution and maturation of lower Paleozoic source rocks in the Tarim Basin, Northwest China," *AAPG Bulletin*, vol. 96, no. 5, pp. 789–821, 2012.

[29] L. Wang, C. Li, and Y. Shi, "Distribution of terrestrial heat flow density in the Tarim Basin," *Acta Geophysica Sinica*, vol. 38, no. 6, pp. 855-856, 1995.

[30] C. G. Feng, S. W. Liu, L. S. Wang, and C. Li, "Present-day geothermal regime in Tarim Basin, Northwest China," *Chinese Journal of Geophysics*, vol. 52, no. 6, pp. 1237–1250, 2009.

[31] H. Yang, G. Zhu, J. Han et al., "Conditions and mechanism of hydrocarbon accumulation in large reef-bank karst oil/gas fields of Tazhong area, Tarim Basin," *Acta Petrologica Sinica*, vol. 27, no. 6, pp. 1865–1885, 2011.

[32] G. Zhu, B. Zhang, H. Yang, J. Su, K. Liu, and Y. Zhu, "Secondary alteration to ancient oil reservoirs by late gas filling in the Tazhong area, Tarim Basin," *Journal of Petroleum Science and Engineering*, vol. 122, pp. 240–256, 2014.

[33] S. Zhang, B. Zhang, H. Yang, G. Zhu, J. Su, and X. Wang, "Adjustment and alteration of hydrocarbon reservoirs during the late Himalayan period, Tarim Basin, NW China," *Petroleum Exploration and Development*, vol. 39, no. 6, pp. 712–724, 2012.

[34] J. Li, Z. Li, N. Qiu, Y. Zuo, J. Yu, and J. Liu, "Carboniferous-Permian abnormal thermal evolution of the Tarim Basin and its implication for deep structure and magmatic activity," *Chinese Journal of Geophysics*, vol. 59, no. 9, pp. 3318–3329, 2016.

[35] H. Li, N. Qiu, Z. Jin, and Z. He, "Geothermal history of Tarim Basin," *Oil & Gas Geology*, vol. 26, no. 5, pp. 613–617, 2005.